Structural basis for multifunctional roles of mammalian aminopeptidase N

Lang Chen, Yi-Lun Lin, Guiqing Peng, and Fang Li[1]

Department of Pharmacology, University of Minnesota Medical School, Minneapolis, MN 55455

Edited by Ralph S. Baric, University of North Carolina, Chapel Hill, NC, and accepted by the Editorial Board September 21, 2012 (received for review June 13, 2012)

Mammalian aminopeptidase N (APN) plays multifunctional roles in many physiological processes, including peptide metabolism, cell motility and adhesion, and coronavirus entry. Here we determined crystal structures of porcine APN at 1.85 Å resolution and its complexes with a peptide substrate and a variety of inhibitors. APN is a cell surface-anchored and seahorse-shaped zinc-aminopeptidase that forms head-to-head dimers. Captured in a catalytically active state, these structures of APN illustrate a detailed catalytic mechanism for its aminopeptidase activity. The active site and peptide-binding channel of APN reside in cavities with wide openings, allowing easy access to peptides. The cavities can potentially open up further to bind the exposed N terminus of proteins. The active site anchors the N-terminal neutral residue of peptides/proteins, and the peptide-binding channel binds the remainder of the peptides/proteins in a sequence-independent fashion. APN also provides an exposed outer surface for coronavirus binding, without its physiological functions being affected. These structural features enable APN to function ubiquitously in peptide metabolism, interact with other proteins to mediate cell motility and adhesion, and serve as a coronavirus receptor. This study elucidates multifunctional roles of APN and can guide therapeutic efforts to treat APN-related diseases.

Mammalian aminopeptidase N (APN) plays pivotal roles in many physiological processes, such as pain sensation, blood pressure regulation, tumor angiogenesis and metastasis, immune cell chemotaxis, sperm motility, cell-cell adhesion, and coronavirus entry (1). Accordingly, APN is a major target for treatment of diseases that are related to the above physiological processes. It is puzzling how APN is able to possess such a wide range of physiological functions, some of which are seemingly unrelated to its aminopeptidase activity. This study determines the atomic structures of mammalian APN and its complexes with a variety of APN-targeting ligands, providing structural basis for the multifunctional roles of APN and for the development of novel therapy strategies to treat APN-related diseases.

The M1-family of metalloenzymes consists of a large number of zinc-dependent aminopeptidases containing a zinc-binding HEXXH motif. As the most extensively studied member in this family, mammalian APN (also known as CD13 or alanine aminopeptidase) is widely expressed on cell surfaces of tissues, such as intestinal epithelia and the nervous system (1). APN preferentially cleaves neutral amino acids, most notably alanine, off the N terminus of peptides. The general catalytic mechanism of M1-family metalloenzymes is believed to be similar to that of prototypic zinc-peptidase thermolysin, which involves catalytic water attacking scissile peptide bonds (2), but detailed catalytic mechanisms of these enzymes remain elusive. To date, crystal structures are available for several members of the M1-family metalloenzymes (3–8). However, these enzymes are monomeric intracellular enzymes with specific physiological roles, whereas mammalian APN is a dimeric cell-surface ectoenzyme with multifunctional roles (1). This study investigates the structural differences between mammalian APN and other M1-family metalloenzymes that account for their functional differences.

Mammalian APN functions ubiquitously in different peptide metabolism pathways. First, APN plays important roles in pain sensation and mood regulation by catalyzing the metabolism of neuropeptides that process sensory information. One of these neuropeptides is enkephalin, which binds to opioid receptors and has pain-relief and mood-regulating effects (9). APN degrades and shortens the in vivo life of enkephalin, and hence enhances pain sensation and regulates mood. Second, APN is involved in blood pressure regulation. APN degrades vasoconstrictive peptide angiotensin-III, causing vasodilation and lowered blood pressure (10). An endogenous APN inhibitor, substance P, blocks both the enkephalin-dependent and angiotensin-dependent pathways (11, 12). Third, APN is overexpressed on the cell surfaces of almost all major cancer forms and is essential for tumor angiogenesis by degrading angiogenic peptides (13). A natural APN inhibitor, bestatin, is a substrate analog for APN and demonstrates antitumor activities (14). Additionally, APN is involved in many other peptide metabolism pathways by catalyzing the degradation of peptides related to these pathways. These peptides include tuftsin, kinins, glutathione, somatostatin, thymopentin, neurokinin A, splenopentin, nociceptin FQ, and more (1). It is not clear how APN is able to access so many peptides from various peptide metabolism pathways.

Curiously, APN also functions in cell motility and adhesion, and many of these functions are seemingly independent of its aminopeptidase activity. For example, APN participates in tumor cell motility as revealed in several studies: stable expression of APN on tumor cell surfaces greatly increases their migratory capacity, and knocking out APN expression or using anti-APN antibodies can block tumor migration (13, 15–17). The mechanisms whereby APN mediates tumor migration have been partially linked to its aminopeptidase activity, as it was shown that APN degrades extracellular matrix proteins (18, 19). However, an unknown activity of APN independent from its aminopeptidase activity also contributes to tumor migration, as suggested by several other studies: APN-mediated tumor migration can be blocked by antibodies that do not target the aminopeptiase activity of APN, and tumor cells expressing an enzymatically inactive APN also show enhanced migration (16, 20). Besides mediating tumor migration, APN also mediates other cell motility processes, such as immune cell chemotaxis and sperm motility (21–25). Additionally, APN mediates cell-cell adhesion by interacting with other cell-surface proteins (16, 26–28). How APN mediates cell motility and adhesion is largely a mystery.

Interestingly, mammalian APN serves as a receptor for coronaviruses, including human respiratory coronavirus 229E (HCoV-

Author contributions: L.C. and F.L. designed research; L.C., Y.-L.L., G.P., and F.L. performed research; L.C., Y.-L.L., G.P., and F.L. analyzed data; and F.L. wrote the paper.

The authors declare no conflict of interest.

This article is a PNAS Direct Submission. R.S.B. is a guest editor invited by the Editorial Board.

Data deposition: The atomic coordinates and structure factors have been deposited in the Protein Data Bank, www.pdb.org (PDB ID codes 4FKE, 4FKF, 4FKH, 4FKK, 4FKN, and 4H5H).

[1]To whom correspondence should addressed. E-mail: lifang@umn.edu.

This article contains supporting information online at www.pnas.org/lookup/suppl/doi:10.1073/pnas.1210123109/-/DCSupplemental.

229E), porcine transmissible gastroenteritis virus (TGEV), feline enteric coronavirus (FCoV), and canine enteric coronavirus (CCoV) (29–31). Coronaviruses are a family of positive-stranded RNA viruses that infect many mammalian and avian species. They exploit diverse cellular receptors for host cell entry through a receptor-binding domain (RBD) on their envelope-anchored spike glycoproteins. Crystal structures are available for several coronavirus receptors, either by themselves or complexed with coronavirus RBDs, illustrating detailed mechanisms whereby these receptors are recognized by coronaviruses (32–37). Mutagenesis has been used to characterize APN/coronavirus interactions, revealing multiple coronavirus-binding sites on APN (38, 39). It is not known how coronavirus binding affects physiological functions of APN.

Here we report the crystal structures of porcine APN and its complexes with peptide substrate poly-alanine, amino acid alanine, substrate analog bestatin, and peptide inhibitor substance P. These structures provide a basis for understanding the multifunctional roles of mammalian APN and for the development of novel therapy strategies to treat APN-related diseases.

Results and Discussion

Structure Determination. After screening APNs from different mammalian species for crystal formation, we found that porcine APN (pAPN) forms crystals suitable for structure determination (Fig. 1 and Table S1). Porcine and human APNs share high sequence identity (Fig. S1) and indistinguishable biochemical and kinetic properties (Table S2). Mammalian APN is a class-II membrane protein comprised of a short intracellular tail, a transmembrane anchor, a small extracellular stalk, and a large ectodomain (Fig. 1*B*). The pAPN ectodomain (residues 62–963) was expressed and purified in insect cells, and subsequently crystallized. The structure of pAPN was determined by a multiple isomorphous-replacement and anomalous-scattering method (MIRAS) using one mercury derivative and one platinum derivative, and was refined at 1.85 Å resolution. Complexes with APN-targeting ligands, including poly-alanine, alanine, bestatin, and substance P, were prepared by soaking each ligand into pAPN crystals. All crystal forms were isomorphous. All of the amino acids of the pAPN ectodomain and every ligand in its entirety could be modeled into electron density (Table S1). Also included in the model were glycans that are *N*-linked to 11 glycosylation sites on pAPN.

Overall Architecture. The general architecture of pAPN ectodomain can be described as seahorse-shaped, with four distinct domains: head, side, body, and tail (Figs. 1, 2*A*, and 3*A*). The zinc-binding active site is located in the body domain (Fig. 3*B*). The head domain (residues 632–963) contains a 16 α-helical superhelix (Fig. S1). The side domain (residues 543–631) adopts a seven-stranded β-sandwich fold. The body domain (residues 281–542) contains two subdomains: N-terminal subdomain (residues 281–369) consists of a five-stranded β-sheet with a connecting α-helix; C-terminal subdomain (residues 370–542) contains a seven α-helical superhelix. The tail domain (residues 62–280) adopts a 15-stranded β-barrel fold. pAPN matches well with other M1-family metalloenzymes in their overall domain arrangements and domain folds (Fig. 2*B*, Fig. S2, and Table S3).

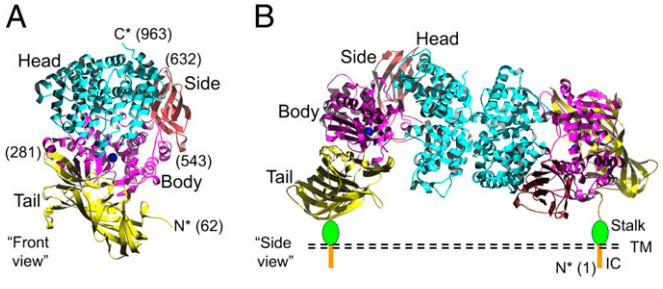

Fig. 1. Overall structure of APN. (*A*) pAPN ectodomain (front view) contains four domains: head (cyan), side (brown), body (magenta), and tail (yellow). (*B*) Structure of dimeric pAPN ectodmain (side view) and model of dimeric full-length pAPN on cell surface. IC, intracellular tail; TM, transmembrane anchor. Residue numbers indicating the locations of domain boundaries are in parenthesis.

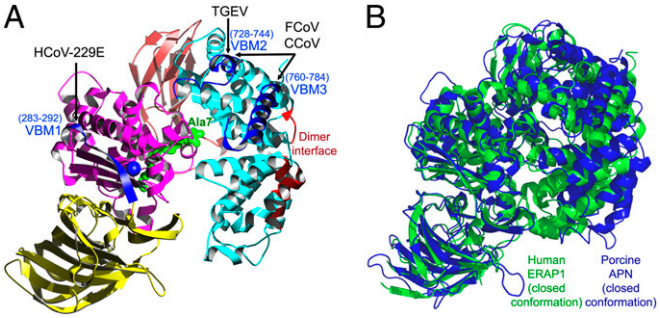

Fig. 2. Spatial distributions of functional regions on APN. (*A*) Spatial relationships among peptide-binding channel, dimerization interface, and coronavirus-binding sites on APN (side view). (*B*) Structural alignment of pAPN (in blue) and human endoplasmic reticulum aminopeptidase-1 (ERAP1) in the closed conformation (in green) (PDB ID code 2YD0).

A unique feature of the pAPN structure is that its zinc-binding active site is located in a spacious cavity with wide openings on three sides (Figs. 2 and 3). This cavity in pAPN is surrounded by its four domains and has a dimension of 50 Å (width), 40 Å (depth), 30 Å (height), and 20 Å (openings). The wide openings of the active-site cavity in pAPN can allow easy access to peptides and other APN-targeting ligands. In comparison, the active sites of other M1-family metalloenzymes are all located in a small and gated compartment (Fig. 2*B* and Fig. S2) (3–6). This structural difference between mammalian APN and other M1-family metalloenzymes is consistent with their different physiological roles: although mammalian APN is a cell-surface ectoenzyme and binds a wide range of peptides required for its multifunctional roles (1), other M1-family metalloenzymes with known structures are intracellular enzymes and only bind a narrow range of peptides required for their specific physiological functions (3–8).

Porcine APN forms head-to-head dimers. Although pAPN was crystallized with one molecule in each asymmetric unit, two pAPN molecules from adjacent asymmetric units form a strong head-to-head dimer by burying 2,000 Å^2 surface area (Fig. 1*B*). Consistent with crystallographic analysis, pAPN exists as a dimer in solution as revealed by dynamic light scattering analysis (Table S4). We therefore construct a model for the overall structure of cell surface-anchored mammalian APN in which the transmembrane anchors of the dimer are physically separated (Fig. 1*B*). This dimer arrangement of pAPN is unique for M1-family metalloenzymes because all other enzymes with known structures are monomers (3–8). The dimer formation of pAPN has functional implications: it can increase the stability of pAPN which, as a cell-surface-anchored ectoenzyme, faces a harsher environment than intracellular proteins. In addition, M1-family metalloenzymes are known to take two distinctive conformations, closed and open, by undergoing hinge-opening movement between its head domain and the rest of its ectodomain. As discussed later, the pAPN structure captured in this study is in a closed conformation. The dimer arrangement of pAPN and the flexibility of the ectodomain/stalk junction appear to facilitate potential conformational changes of APN.

Peptide Binding. The charge distribution map of pAPN shows a negatively charged channel leading to the zinc-binding active site

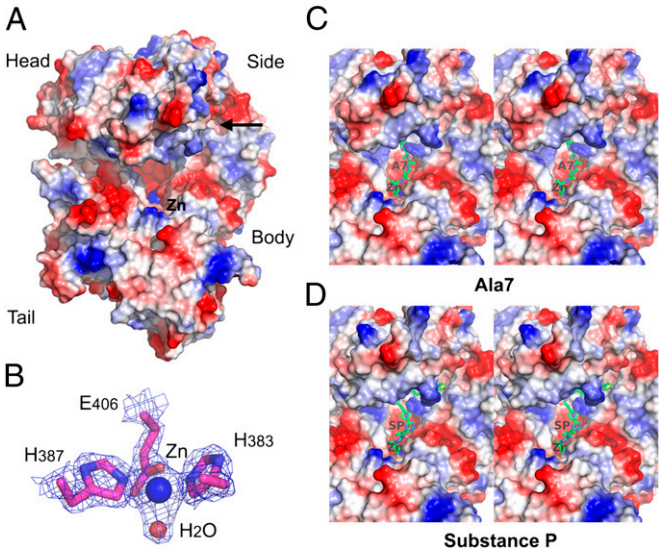

Fig. 3. Peptide-binding channel in APN. (*A*) Charge distribution of pAPN ectodomain (front view). Positive and negative charges are blue and red, respectively. Unit of distances is in angstroms. Zinc is shown as a blue ball. Arrow points to entrance site of peptides. (*B*) Electron density map of zinc-binding site at 5.0 σ. (*C* and *D*) Stereo images showing the binding of Ala7 (A7) and substance P (SP) (both in green) to pAPN.

(Fig. 3*A*). The channel is formed primarily between the head and body domains, although the entrance of the channel also involves the side domain. Substrate poly-alanine (Alanine7 or Ala7) has its N-terminal residue anchored to the active site and the rest of the peptide bound to the channel (Fig. 3*C*). Substance P (RPKPQQFFGLM) also binds to this channel (Fig. 3*D*). The structure of substance P shows an extended conformation similar to Ala7. The binding paths of Ala7 and substance P overlap, except that substance P is longer. The distance between the C terminus of substance P and the entrance of the channel is about 7 Å, which can accommodate another two residues. Therefore, the peptide-binding channel spans ~13 amino acids when peptides are in extended conformations.

Detailed interactions between pAPN and peptides reveal several structural features of APN that define its substrate preferences. First, Gln208, Glu350, and Glu406 from pAPN form three hydrogen bonds with the free N-terminal amine group of peptides and other APN-targeting ligands, such as amino acids and bestatin (Fig. 4). These interactions firmly anchor the N terminus of peptides to the active site for catalysis, and define APN as an N-terminal exo-aminopeptidase. Second, Met349 from pAPN forms a hydrophobic interaction with C_β of the N-terminal amino acid of peptides (Fig. 4 *A* and *C*). This interaction helps explain why alanine is preferred by APN in the N-terminal position of peptide substrates. Third, despite extensive interactions with the N-terminal residue of peptides, APN binds the rest of the peptides mainly through hydrogen bonds with peptide main-chain groups (Fig. 4 *C* and *D*). These interactions are less dependent on peptide sequences, allowing APN to bind peptides of a wide range of sequences. Our study helps clarify some of the long-standing puzzles over the substrate preferences of APN.

Catalytic Mechanism. We propose the following catalytic mechanism for mammalian APN based on structural analysis of pAPN and structural comparisons of pAPN to prototypic zinc-peptidase thermolysin (2). In pAPN, zinc is chelated by three residues Glu406, His383, and His387 (Fig. 3*B*). A catalytic water is activated by zinc, is positioned by Glu350, and is ready to transfer a proton to Glu384 (Figs. 3*B* and 5*A*). After the peptide substrate enters, the active site arrangement remains the same, and the carbonyl oxygen and nitrogen of the scissile peptide bond of the substrate are activated by zinc/Tyr472 and the carbonyl oxygen of Ala348, respectively (Fig. 5*B*). Subsequently, the catalytic water attacks the carbonyl carbon of the scissile peptide bond, and Glu384 shuttles a proton from the catalytic water to the leaving nitrogen group (Fig. 5*B*). Finally, the peptide bond is hydrolyzed.

To support the above proposed catalytic mechanism of APN, mutagenesis and biochemical assays were performed. First, we made three pAPN mutants, all of which show vastly decreased catalytic activities (Fig. 5*F*). Mutation E384Q likely interferes with proton transfer from the catalytic water to the leaving nitrogen group, mutation E350Q likely puts the catalytic water in a nonoptimal position for catalysis, and mutation Y472F likely leads to an insufficiently activated scissile peptide bond. Second, we performed pH-dependent enzymatic assays for both human and porcine APNs (Fig. S3). The results show that APN functions best at neutral or slightly basic pH, consistent with the pH of APN-expressing tissues, such as the nervous system or the intestines.

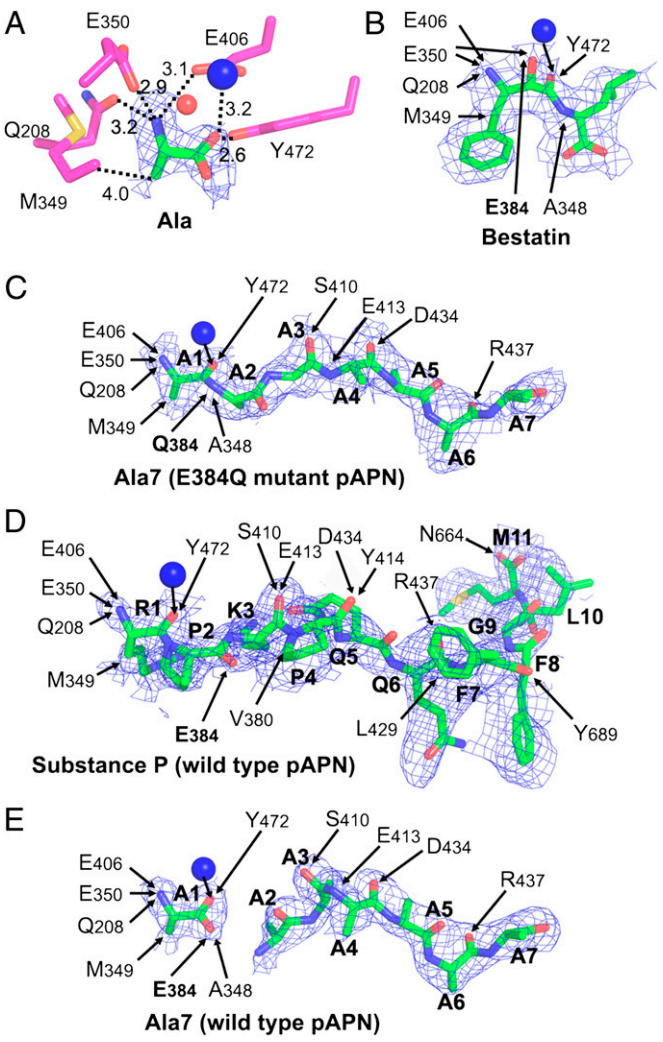

Fig. 4. Detailed interactions between APN and APN-targeting ligands. The ligands include: (*A*) alanine (Ala) bound to wild type pAPN; (*B*) bestatin bound to wild-type pAPN; (*C*) poly-alanine (Ala7) bound to E384Q mutant pAPN; (*D*) substance P bound to wild type pAPN; (*E*) Ala7 bound to wild-type pAPN where Ala7 has been degraded in the crystal. Unit of distances is in angstroms. Zinc is shown as a blue ball and catalytic water as a red ball. The electron densities correspond to 2Fo-Fc omit maps contoured at 1.0 σ.

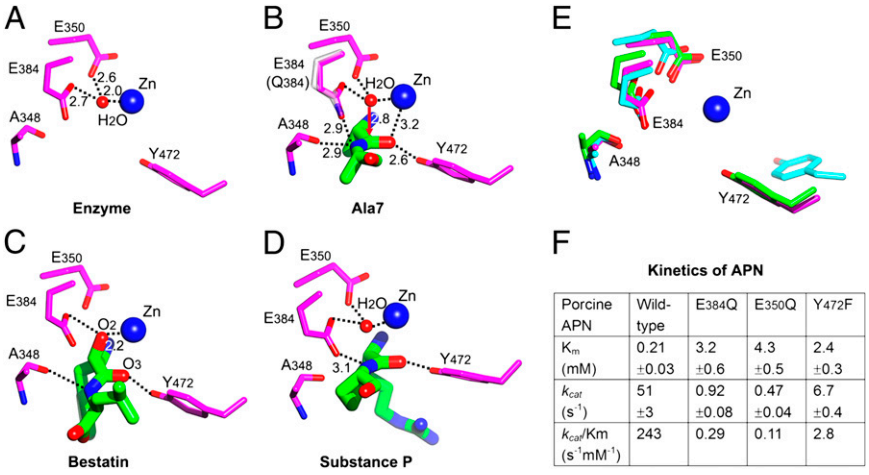

F

Kinetics of APN

Porcine APN	Wild-type	E384Q	E350Q	Y472F
K_m (mM)	0.21 ±0.03	3.2 ±0.6	4.3 ±0.5	2.4 ±0.3
k_{cat} (s^{-1})	51 ±3	0.92 ±0.08	0.47 ±0.04	6.7 ±0.4
k_{cat}/Km ($s^{-1}mM^{-1}$)	243	0.29	0.11	2.8

Fig. 5. Catalytic mechanism of APN. (*A*) Active site arrangement in pAPN. (*B*) Interactions between catalytic residues of pAPN (magenta) and scissile peptide bond of Ala7 (green). Although Gln384 (white) was introduced to pAPN to generate a catalytically incompetent enzyme for crystallographic studies, Glu384 (magenta) from wild-type pAPN was grafted here to illustrate the catalytic mechanism of APN. (*C*) Interactions between catalytic residues of pAPN and bestatin. (*D*) Interactions between catalytic residues of pAPN and substance P. (*E*) pAPN is in the closed and catalytically active conformation based on its active site arrangement. Shown is the structural alignment of the active sites of pAPN (in magenta), ERAP1 in an open and catalytically inactive conformation (in cyan; PDB ID code 3QNF), and ERAP1 in a closed and catalytically active conformation (in green; PDB ID code 2YD0). (*F*) Kinetics of pAPN and its catalytically incompetent mutants.

Moreover, APN activity becomes very low at further increased pH, likely because of deprotonation of catalytic and substrate-binding tyrosines (e.g., Tyr472), whereas APN activity becomes completely lost at low pH, likely because of protonation of catalytic and substrate-binding histidines, glutamates, and aspartates (e.g., Glu384). Extremely low or high pH may also have profound impact on the overall structure and conformation of the enzyme. Overall, these data support the active site arrangement, assigned roles of catalytic residues, and proposed proton transfer pathway in pAPN catalysis.

Our study on pAPN has implications for other M1-family metalloenzymes. First, it readily explains the mechanism of inhibition of bestatin on M1-family metalloenzymes, which has not been accurately addressed before: the O_2 group of bestatin displaces catalytic water and stalls the catalysis (Fig. 5*C*). Second, this study explains why peptides with a proline in the second position to the N terminus cannot be easily degraded by M1-family metalloenzymes. As in the case of substance P, the leaving nitrogen group of Pro2 cannot form a hydrogen bond with pAPN Ala348 for lack of protons, and hence the scissile peptide bond is insufficiently activated (Fig. 5*D*). Third, it helps understand previous studies on other M1-family metalloenzymes. The previously available structures in the family were either of proteins alone or complexed with bestatin (3–6); only mammalian leukotriene A4 hydrolase was crystallized with a three-residue peptide, but the conformation of the peptide was catalytically inactive because the free N-terminal amine group of the peptide displaces catalytic water (Fig. S4) (7, 8). Understanding the catalytic mechanisms of M1-family metalloenzymes can help develop inhibitors against these physiologically and medically important enzymes.

Enzyme Conformation and Catalytic Cycle. M1-family metalloenzymes are known to take two distinct conformations: a closed and catalytically active conformation and an open and catalytically inactive conformation. The pAPN structure captured in our study is in the closed and catalytically active conformation: Ala7 substrate remains intact in E384Q mutant pAPN crystals (Fig. 4*C*), but has been degraded in wild-type pAPN crystals, generating two products alanine and Ala6. (Fig. 4*E*). For the next cycle of aminopeptidase reaction, the enzyme would have to switch to the open and catalytically inactive conformation, rearrange its catalytic residues including Tyr472 (Fig. 5*E*), release product alanine, and allow the other product Ala6 to translocate into the active site to become the next substrate. However, because of the fixed crystal lattices in our study, pAPN cannot switch to the open conformation or rearrange its catalytic residues. As a result, product alanine from the first cycle of aminopeptidase reaction is trapped in the active site by catalytic residues including Tyr472, preventing the next cycle of aminopeptidase reaction from happening. These results present direct evidence for the closed and catalytically active conformation of our pAPN structure.

Protein Binding. Our study suggests that pAPN can potentially further open up its active-site cavity and peptide-binding channel to bind exposed N terminus of proteins that would not be accessible to pAPN in the closed conformation. To test this hypothesis, we investigated the interactions between mammalian APNs and TNF-α (exposed N terminus is eight-residues long) or GST (exposed N terminus is two-residues long) (Fig. S5 *A* and *B*). Our results show that both porcine and human APNs have significantly higher affinity for TNF than for GST (Fig. 6*A*). The interactions between TNF and APNs can be inhibited by substance P and alanine, suggesting that the exposed N terminus of TNF competes with substance P for the APN peptide-binding channel and with alanine for the APN active site. Hence, the exposed N terminus of proteins can bind to APN in the same way as peptides do, and the length of the exposed N terminus of the proteins appears to be a limiting factor for their APN-binding affinity. Because the length of the peptide-binding channel of APN is roughly 13 residues, TNF does not fit into the pAPN structure in the closed conformation. Instead, TNF can only bind APN in the open conformation (Fig. 6*B*). These results suggest that cell surface-anchored APN has the potential to interact with the exposed N terminus of some extracellular matrix proteins and cell-surface proteins. Thus, APN can partner with these proteins to perform its seemingly mysterious functions in cell motility and adhesion.

Signal transduction has been proposed as a function of APN. However, the intracellular tail of APN is short and does not contain any known signaling motif. Thus, it is believed that APN regulates the signal transduction functions of its protein partners with unknown identity (1, 40, 41). In light of our characterization of protein-binding capacity of APN, we model potential conformational changes of dimeric APN on the cell membrane that may be relevant to signal transduction (Fig. S5 *C* and *D*). Based on this model, throughout the closed-to-open conformational changes of APN, the dimer interface between APN head domains is maintained, the two membrane anchors move further apart from each other, and the overall APN structure is drawn closer to the cell membrane. These potentially significant structural changes of dimeric APN may regulate the structures and functions of its protein partners and contribute to signal transduction. This model merits further investigation.

Coronavirus Binding. We have mapped known coronavirus-binding sites to the pAPN structure (Fig. 2*A*), based on previously published mutagenesis data (38, 39). Coronavirus-binding sites cluster

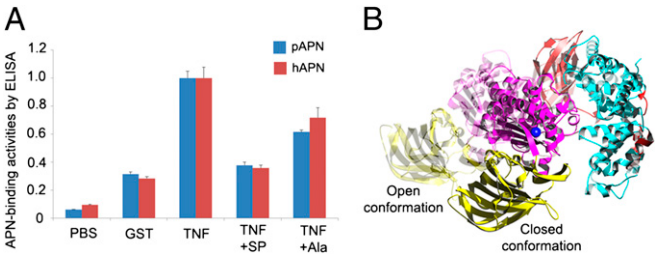

Fig. 6. Interactions between APN and proteins. (*A*) APN-binding activities of TNF-α and GST as measured by ELISA. TNF/APN binding was carried out either in the absence of inhibitors or in the presence of substance P (SP) or alanine. All of the measured binding activities have been calibrated against TNF/pAPN binding. (*B*) Potential conformational changes of APN. The pAPN structure captured in this study is in a closed conformation, but can potentially switch to an open conformation to interact with the N terminus of proteins.

into three regions, which we term "virus-binding motifs" (VBMs). VBM1 (residues 283–292) is a β-strand turn in the body domain, whereas VBM2 (residues 728–744) and VBM3 (residues 760–784) are both α-helix turns in the head domain. HCoV-229E recognizes VBM1, TGEV recognizes VBM2, and FCoV and CCoV recognize both VBM2 and VBM3. All three VBMs are located on the outside surface of APN and easily accessible to viruses. Moreover, coronavirus binding does not appear to interfere with the physiological functions of APN, as the VBMs do not block the peptide-binding path or overlap with the dimer interface. Apparently, coronaviruses have evolved a mechanism to use APN as their cell entry receptor without interfering with the physiological functions of this important host enzyme.

Multifunctional Roles and Therapeutic Implications. How does APN function as a multifunctional enzyme? To address this question, we have determined crystal structures of porcine APN and its complexes with a variety of APN-targeting ligands. APN is a seahorse-shaped molecule and forms head-to-head dimers. Its active site and peptide-binding channel are located in cavities with wide openings and are thus easily accessible to peptides. The active site firmly anchors the N-terminal neutral residue of peptides, and the peptide-binding channel binds the remainder of the peptides in a sequence-independent fashion. Consequently, APN functions ubiquitously in peptide metabolism, degrading a wide spectrum of peptides that are involved in pain sensation, mood regulation, blood pressure regulation, angiogenesis, and many other physiological processes. Although the APN structure captured in this study is in a closed and catalytically active conformation, APN can potentially switch to an open conformation and bind the exposed N terminus of some extracellular matrix proteins and cell-surface proteins. Consequently, APN can partner with these proteins and function in cell motility and adhesion. Furthermore, APN provides an exposed outer surface for coronavirus binding, without interruption of its physiological functions or dimeric structure. These above structural features define APN as a multifunctional enzyme.

Our study can guide structure-based development of APN-targeting ligands, including substrate analog inhibitors, peptide inhibitors, and antibodies. Many APN-targeting ligands have been discovered or developed, some of which are currently used clinically or in clinical trials (14). However, because of the lack of atomic structures of APN in the past, development of efficient APN-targeting ligands had been severely hindered. This study provides detailed structural information about the APN active site, peptide-binding channel, and APN/ligand interactions, which can guide development of novel APN-targeting substrate analogs and peptide inhibitors with high affinity and selectivity for APN. It is worth noting that many of the currently available APN-targeting inhibitors can also inhibit other M1-family metalloenzymes (14), and such lack of specificity causes adverse side effects (42). Hence, it is imperative to develop inhibitors with higher specificity for APN through structure-based rational design. In addition, antibodies that target coronavirus-binding sites on APN can potentially block coronavirus infections, without interfering with the physiological functions of APN. Therefore, our study provides a structural framework for development of APN-targeting inhibitors or antibodies to treat or cure APN-related diseases, such as pain, mood disorder, abnormal blood pressure, cancer, immune disorder, and virus infection, all of which pose major threats to human health.

Recently Published Structural Studies of Mammalian APN. During the review process of our study, two studies were published reporting the structures of mammalian APN. Although related, our study's scope goes significantly beyond these recent publications. One study described the structure of coronavirus-RBD–bound pAPN (43). Unlike the present study, that study focused on coronavirus/APN interactions rather than the multifunctional roles of APN. The second study described the structure of human APN complexed with peptide angiontensin-III and inhibitors bestatin and amastatin, focusing on the peptide- and inhibitor-binding modes of APN (44). However, the second study did not address detailed catalytic mechanism of APN. First, all of the crystallizations were done at pH 5.0, under which APN has no enzymatic activities (Fig. S3). Second, catalytic water was not observed in any of the structures. Third, the peptide-bound APN was depleted of zinc before crystallization. Therefore, the second study lacked direct experimental evidence for APN catalysis. Our study was done under physiologically relevant pH and all of the catalytic elements, including catalytic water, zinc, catalytic residues, and peptide substrate, were in position for APN catalysis, and thus it provides direct and comprehensive evidence for the catalytic mechanism of APN. In addition, our study elucidates the peptide- and protein-binding mechanisms of APN, as well as the spatial relationship between coronavirus-binding sites and substrate-binding channel in APN. Importantly, our study correlates these mechanisms to the multifunctional roles of APN, and these findings and observations are unique to date.

Materials and Methods

Structure Determination. Porcine APN ectodomain (residues 62–963) was expressed and purified as previously described (35). Briefly, pAPN containing N-terminal honey bee-melittin signal peptide and C-terminal His6 tag was expressed in insect cells and purified sequentially on Ni-NTA column and gel-filtration column. pAPN was concentrated to 10 mg/mL in buffer containing 20 mM Tris pH 7.2 and 200 mM NaCl. Crystallization of pAPN was set up by hand, with 1 μL protein solution and 1 μL well solution containing 18% (wt/vol) PEG3350, 200 mM Li_2SO_4, and 100 mM Hepes pH 7.2 mixed together in sitting drops. Crystals of pAPN were grown at 4 °C. Crystals first showed up in 2 d and were allowed to grow for another 2 wk before they were harvested in crystal freezing buffer containing 20% ethylene glycol, 25% PEG3350, 200 mM Li_2SO_4, and 100 mM Hepes pH 7.2. The crystals were then flash-frozen in liquid N_2 and used for data collection.

To prepare heavy-atom derivatives and pAPN/ligand complexes, crystals of pAPN were soaked for 2 d in soaking buffer containing 1 mM heavy atom or 5 mM ligand, 20% (vol/vol) ethylene glycol, 25% PEG3350, 200 mM Li_2SO_4, and 100 mM Hepes pH 7.2. The heavy atom ($EthylHgPO_4$ or K_2PtCl_6) or ligand (alanine, bestatin, poly-alanine, or substance P) was first dissolved in water to make 100-mM stock solution and then diluted in the crystal freezing buffer containing 20% ethylene glycol, 25% PEG3350, 200 mM Li_2SO_4, and 100 mM Hepes pH 7.2. From Hg-derivatized and Pt-derivatized crystals, 6 Hg sites and 12 Pt sites were identified, respectively. MIRAS phases were calculated. Solvent flattening was performed. A model of pAPN was built and refined. Models of the ligands were built based on difference maps. Table S1 lists all crystallographic procedures and used software.

Molecular Weight Measurement. Dynamic light scattering (DLS) was carried out to measure the molecular weight of pAPN ectodomain in solution using DLS machine DynaPro NanoStar (Wyatt Technology). The measurement was performed at 25 °C on 3 mg/mL pAPN ectodomain in buffer containing 20 mM Tris (pH 7.2) and 200 mM NaCl, and was repeated four times. Data were analyzed using software Dynamics 7.1.7.

APN Activity Assays. APN activity was determined at 1 nM enzyme concentration in 100 μL 60 mM KH_2PO_4 buffer at pH 7.2, with alanine-p-nitroanilide (Sigma-Aldrich) as substrate in gradient concentrations from 100 μM to 10 mM. APN and substrate were incubated at 37 °C for 60 min. Formation of product p-nitroanilide was measured using spectrophotometer at 405 nm.

Protein Binding Assays by ELISA. ELISA was used to characterize the binding of GST and TNF to porcine and human APNs, as previously described (35). Briefly, 100 μg/mL APN with C-terminal Fc tag was coated in 96-well plates (Nunc). The plates were then sequentially incubated with BSA, 1 μM GST or TNF containing C-terminal His6 tag, anti-His antibody (Invitrogen), HRP-conjugated goat–anti-mouse IgG antibody, and Femto-ELISA-HRP substrates. The reaction was stopped with 1 N HCl, and the absorbance of the resulting yellow color was read at 450 nm. To inhibit protein bindings, 100 μM substance P or 50 mM alanine was added before GST or TNF was added to the plates.

ACKNOWLEDGMENTS. We thank Carrie Wilmot, Weikai Li, Stanley Thayer, Hiroshi Hiasa, Robert Geraghty, and Joseph Pasquarella for discussion and comments, Kathryn Holmes for the porcine aminopeptidase N gene, Lokesh Gakhar for assistance in dynamic light-scattering experiments, and the staff at the Advanced Photon Source beamlines 19-ID and 24-ID for assistance in X-ray data collection. Computer resources were provided by the Basic Sciences Computing Laboratory of the University of Minnesota Supercomputing Institute. This work was supported by National Institutes of Health Grant R01AI089728 (to F.L.).

1. Mina-Osorio P (2008) The moonlighting enzyme CD13: Old and new functions to target. *Trends Mol Med* 14(8):361–371.
2. Lipscomb WN, Sträter N (1996) Recent advances in zinc enzymology. *Chem Rev* 96(7): 2375–2434.
3. Kochan G, et al. (2011) Crystal structures of the endoplasmic reticulum aminopeptidase-1 (ERAP1) reveal the molecular basis for N-terminal peptide trimming. *Proc Natl Acad Sci USA* 108(19):7745–7750.
4. McGowan S, et al. (2009) Structural basis for the inhibition of the essential *Plasmodium falciparum* M1 neutral aminopeptidase. *Proc Natl Acad Sci USA* 106(8):2537–2542.
5. Nguyen TT, et al. (2011) Structural basis for antigenic peptide precursor processing by the endoplasmic reticulum aminopeptidase ERAP1. *Nat Struct Mol Biol* 18(5):604–613.
6. Addlagatta A, Gay L, Matthews BW (2006) Structure of aminopeptidase N from *Escherichia coli* suggests a compartmentalized, gated active site. *Proc Natl Acad Sci USA* 103(36):13339–13344.
7. Tholander F, et al. (2008) Structure-based dissection of the active site chemistry of leukotriene A4 hydrolase: Implications for M1 aminopeptidases and inhibitor design. *Chem Biol* 15(9):920–929.
8. Thunnissen MM, Nordlund P, Haeggström JZ (2001) Crystal structure of human leukotriene A(4) hydrolase, a bifunctional enzyme in inflammation. *Nat Struct Biol* 8(2): 131–135.
9. König M, et al. (1996) Pain responses, anxiety and aggression in mice deficient in preproenkephalin. *Nature* 383(6600):535–538.
10. Danziger RS (2008) Aminopeptidase N in arterial hypertension. *Heart Fail Rev* 13(3): 293–298.
11. Datar P, Srivastava S, Coutinho E, Govil G (2004) Substance P: Structure, function, and therapeutics. *Curr Top Med Chem* 4(1):75–103.
12. Xu Y, Wellner D, Scheinberg DA (1995) Substance P and bradykinin are natural inhibitors of CD13/aminopeptidase N. *Biochem Biophys Res Commun* 208(2):664–674.
13. Bauvois B (2004) Transmembrane proteases in cell growth and invasion: New contributors to angiogenesis? *Oncogene* 23(2):317–329.
14. Bauvois B, Dauzonne D (2006) Aminopeptidase-N/CD13 (EC 3.4.11.2) inhibitors: Chemistry, biological evaluations, and therapeutic prospects. *Med Res Rev* 26(1): 88–130.
15. Carl-McGrath S, Lendeckel U, Ebert M, Röcken C (2006) Ectopeptidases in tumour biology: A review. *Histol Histopathol* 21(12):1339–1353.
16. Chang YW, et al. (2005) CD13 (aminopeptidase N) can associate with tumor-associated antigen L6 and enhance the motility of human lung cancer cells. *Int J Cancer* 116(2): 243–252.
17. Hashida H, et al. (2002) Aminopeptidase N is involved in cell motility and angiogenesis: Its clinical significance in human colon cancer. *Gastroenterology* 122(2):376–386.
18. Menrad A, Speicher D, Wacker J, Herlyn M (1993) Biochemical and functional characterization of aminopeptidase N expressed by human melanoma cells. *Cancer Res* 53 (6):1450–1455.
19. Saiki I, et al. (1993) Role of aminopeptidase N (CD13) in tumor-cell invasion and extracellular matrix degradation. *Int J Cancer* 54(1):137–143.
20. Fukasawa K, et al. (2006) Aminopeptidase N (APN/CD13) is selectively expressed in vascular endothelial cells and plays multiple roles in angiogenesis. *Cancer Lett* 243(1): 135–143.
21. Carlsson L, Ronquist G, Eliasson R, Egberg N, Larsson A (2006) Flow cytometric technique for determination of prostasomal quantity, size and expression of CD10, CD13, CD26 and CD59 in human seminal plasma. *Int J Androl* 29(2):331–338.
22. Irazusta J, et al. (2004) Enkephalin-degrading enzymes in normal and subfertile human semen. *J Androl* 25(5):733–739.
23. González Buitrago JM, Navajo JA, García Diez LC, Herruzo A (1985) Seminal plasma leucine aminopeptidase in male fertility. *Andrologia* 17(2):139–142.
24. Tani K, et al. (2000) CD13/aminopeptidase N, a novel chemoattractant for T lymphocytes in pulmonary sarcoidosis. *Am J Respir Crit Care Med* 161(5):1636–1642.
25. Shimizu T, et al. (2002) CD13/aminopeptidase N-induced lymphocyte involvement in inflamed joints of patients with rheumatoid arthritis. *Arthritis Rheum* 46(9): 2330–2338.
26. Mina-Osorio P, et al. (2008) CD13 is a novel mediator of monocytic/endothelial cell adhesion. *J Leukoc Biol* 84(2):448–459.
27. Mina-Osorio P, Shapiro LH, Ortega E (2006) CD13 in cell adhesion: Aminopeptidase N (CD13) mediates homotypic aggregation of monocytic cells. *J Leukoc Biol* 79(4):719–730.
28. Salmi M, Jalkanen S (2005) Cell-surface enzymes in control of leukocyte trafficking. *Nat Rev Immunol* 5(10):760–771.
29. Yeager CL, et al. (1992) Human aminopeptidase N is a receptor for human coronavirus 229E. *Nature* 357(6377):420–422.
30. Delmas B, et al. (1992) Aminopeptidase N is a major receptor for the entero-pathogenic coronavirus TGEV. *Nature* 357(6377):417–420.
31. Tresnan DB, Levis R, Holmes KV (1996) Feline aminopeptidase N serves as a receptor for feline, canine, porcine, and human coronaviruses in serogroup I. *J Virol* 70(12): 8669–8674.
32. Li F, Li WH, Farzan M, Harrison SC (2005) Structure of SARS coronavirus spike receptor-binding domain complexed with receptor. *Science* 309(5742):1864–1868.
33. Tan KM, et al. (2002) Crystal structure of murine sCEACAM1a[1,4]: A coronavirus receptor in the CEA family. *EMBO J* 21(9):2076–2086.
34. Wu KL, Li WK, Peng GQ, Li F (2009) Crystal structure of NL63 respiratory coronavirus receptor-binding domain complexed with its human receptor. *Proc Natl Acad Sci USA* 106(47):19970–19974.
35. Peng GQ, et al. (2011) Crystal structure of mouse coronavirus receptor-binding domain complexed with its murine receptor. *Proc Natl Acad Sci USA* 108(26): 10696–10701.
36. Towler P, et al. (2004) ACE2 X-ray structures reveal a large hinge-bending motion important for inhibitor binding and catalysis. *J Biol Chem* 279(17):17996–18007.
37. Li F (2012) Evidence for a common evolutionary origin of coronavirus spike protein receptor-binding subunits. *J Virol* 86(5):2856–2858.
38. Tusell SM, Schittone SA, Holmes KV (2007) Mutational analysis of aminopeptidase N, a receptor for several group 1 coronaviruses, identifies key determinants of viral host range. *J Virol* 81(3):1261–1273.
39. Wentworth DE, Holmes KV (2001) Molecular determinants of species specificity in the coronavirus receptor aminopeptidase N (CD13): Influence of N-linked glycosylation. *J Virol* 75(20):9741–9752.
40. Santos AN, Langner J, Herrmann M, Riemann D (2000) Aminopeptidase N/CD13 is directly linked to signal transduction pathways in monocytes. *Cell Immunol* 201(1): 22–32.
41. Navarrete Santos A, Roentsch J, Danielsen EM, Langner J, Riemann D (2000) Aminopeptidase N/CD13 is associated with raft membrane microdomains in monocytes. *Biochem Biophys Res Commun* 269(1):143–148.
42. Mishima Y, et al. (2007) Continuous treatment of bestatin induces anti-angiogenic property in endothelial cells. *Cancer Sci* 98(3):364–372.
43. Reguera J, et al. (2012) Structural bases of coronavirus attachment to host aminopeptidase N and its inhibition by neutralizing antibodies. *PLoS Pathog* 8(8):e1002859.
44. Wong AHM, Zhou D, Rini JM (2012) The X-ray crystal structure of human aminopeptidase N reveals a novel dimer and the basis for peptide processing. *J Biol Chem*, in press.